Received: 28 June 2020 | Revised: 18 September 2020 | Accepted: 12 October 2020

DOI: 10.1002/jdn.10071

RESEARCH ARTICLE

INTERNATIONAL JOURNAL OF DEVELOPMENTAL NEUROSCIENCE

WILEY

Quantitative analyses of high-angular resolution diffusion imaging (HARDI)-derived long association fibers in children with sensorineural hearing loss

Tadashi Shiohama[1,2] | **Brianna Chew**[3] | **Jacob Levman**[1,4] | **Emi Takahashi**[1]

[1]Division of Newborn Medicine, Department of Medicine, Boston Children's Hospital, Harvard Medical School, Boston, MA, USA

[2]Department of Pediatrics, Chiba University Hospital, Chiba, Japan

[3]College of Science, Northeastern University, Boston, MA, USA

[4]Department of Mathematics, Statistics and Computer Science, St. Francis Xavier University, Antigonish, NS, Canada

Correspondence
Tadashi Shiohama, Department of Pediatrics, Chiba University Hospital, 1-8-1 Inohana, Chuo-ku, Chiba-shi, Chiba 260-8670, Japan.
Email: asuha_hare@yahoo.co.jp

Funding information
This research project was supported by National Institutes of Health (R01HD078561, R21MH118739, R21HD098606, and R03NS101372) to E.T., Natural Science and Engineering Research Council of Canada's Canada Research Chair grant (231266), a Canada Foundation for Innovation and Nova Scotia Research and Innovation Trust infrastructure grant (R0176004), and a St. Francis Xavier University research startup grant (R0168020) to J.L

Abstract

Sensorineural hearing loss (SNHL) is the most common developmental sensory disorder due to a loss of function within the inner ear or its connections to the brain. While successful intervention for auditory deprivation with hearing amplification and cochlear implants during a sensitive early developmental period can improve spoken-language outcomes, SNHL patients can suffer several cognitive dysfunctions including executive function deficits, visual cognitive impairment, and abnormal visual dominance in speaking perception even after successful intervention. To evaluate whether long association fibers are involved in the pathogenesis of impairment on the extra-auditory cognitive process in SNHL participants, we quantitatively analyzed high-angular resolution diffusion imaging (HARDI) tractography-derived fibers in participants with SNHL. After excluding cases with congenital disorders, perinatal brain damage, or premature birth, we enrolled 17 participants with SNHL aged under 10 years old. Callosal pathways (CP) and six types of cortico-cortical association fibers (arcuate fasciculus [AF], inferior longitudinal fasciculus [ILF], inferior fronto-occipital fasciculus [IFOF], uncinate fasciculus [UF], cingulum fasciculus [CF], and fornix [Fx]) in both hemispheres were identified and visualized. The ILF and IFOF were partly undetected in three profound SNHL participants. Compared to age- and gender-matched neurotypical controls (NC), decreased volumes, increased lengths, and high apparent diffusion coefficient (ADC) values without difference in fractional anisotropy (FA) values were identified in multiple types of fibers in the SNHL group. The impairment of long association fibers in SNHL may partly be related to the association of cognitive dysfunction with SNHL.

KEYWORDS

apparent diffusion coefficient, fractional anisotropy, high-angular resolution diffusion imaging, long association fibers, sensorineural hearing loss

Abbreviations: ADC, apparent diffusion coefficient; AF, arcuate fasciculus; CC, corpus callosum; CF, cingulum fasciculus; CP, callosal pathways; DTI, diffusion tensor imaging; FA, fractional anisotropy; Fx, fornix; HARDI, high-angular resolution diffusion imaging; IFOF, inferior fronto-occipital fasciculus; ILF, inferior longitudinal fasciculus; MRI, magnetic resonance imaging; NC, neurotypical controls; SNHL, sensorineural hearing loss; TBSS, tract-based spatial statistics; UF, uncinate fasciculus; YO, years old.

1 | INTRODUCTION

Sensorineural hearing loss (SNHL) is the most common developmental sensory disorder due to a loss of function within the inner ear or its connections to the brain (Martines et al., 2013). SNHL in childhood is mainly caused by cochlear dysfunction due to genetic syndromes, congenital infections, and meningitis (Kral & O'Donoghue, 2010). Auditory deprivation at the fetal period affects neurocognitive functions via the decrease of auditory input or the secondary restriction of social communications (Kral et al., 2016). Even after successful intervention, children with congenital hearing loss can suffer several cognitive dysfunctions including executive function deficits (Kronenberger et al., 2014), visual cognitive impairment (Dye, 2014; Dye & Hauser, 2014; Turgeon et al., 2012), and abnormal visual dominance in speaking perception (Bergeson et al., 2010; Buckley & Tobey, 2011) as well as language delay (Tomblin et al., 2015; Yoshinaga-Itano et al., 2017).

The cochlear function and afferent auditory pathway are established from 23 to 26 weeks after conception (Kral et al., 2016), which precedes the sulcation of the ventral and lateral surface (Garel et al., 2003). Auditory input during the fetal period modulates human brain development (Berger et al., 2017; Kral, 2013; Kral et al., 2016; Kral & O'Donoghue, 2010). Therefore, hearing deprivation in utero would disturb functional maturation, delay cortical synaptogenesis, and increase subsequent synaptic elimination (Kral, 2013; Kral et al., 2016; Kral & O'Donoghue, 2010). A pathohistological study showed that congenital SNHL affects the deep layer of the primary and secondary auditory cortex in human patients and animal models (Berger et al., 2017). In addition, the primary auditory area has functional connections with the primary visual area in humans (Petro et al., 2017; Raij et al., 2010; Vetter et al., 2014; Watanabe et al., 2013). These reports may explain why broad cognitive dysfunctions are observed in SNHL patients.

To identify the structural changes in auditory and cognitive dysfunctions in children and adults with SNHL, several neuroimaging studies have been carried out, and have shown that decreased thickness in the left lateral occipital cortex (Shiohama et al., 2019a), can be observed in SNHL children. On the contrary, several studies have reported that the auditory area in SNHL patients was innervated by other sensory systems (Lomber et al., 2010; Sadato et al., 2005). Interestingly, prior structural MRI studies have independently observed that volumes of gray matter in auditory areas are preserved in SNHL (Hribar et al., 2014; Li et al., 2012; Shibata, 2007; Shiohama et al., 2019a).

In contrast to cortical morphometry studies using T1-weighted images, there are only a few studies concerning diffusion MRI in children with SNHL (Chang et al., 2012; Jiang et al., 2019; Park et al., 2018; Wang, Chen, et al., 2019; Wang, Liang, et al., 2019; Wu et al., 2016). These studies mainly focus on fractional anisotropy (FA) values in auditory pathways (lemniscus lateralis, inferior colliculus, medial geniculate bodies, and auditory radiations) and speech composition centers (e.g., Broca's gyrus, and Heschl's gyrus), and there is no quantitative study of tractography-based long association fibers to our best knowledge. Hence, whether and how long association fibers are affected in congenital SNHL still remains unclear. The long association fibers play a key role in intellectual abilities such as speech and language processing (Friederici, 2015), arithmetic processing (McCaskey et al., 2020), motor imagery processing (Oostra et al., 2016), and cognitive functions (Filley & Fields, 2016). The aim of this study is to investigate the pathogenesis of nonverbal cognitive dysfunction in SNHL by quantitatively analyzing long association fibers in children with SNHL.

2 | PATIENTS AND METHODS

2.1 | Patients

We reviewed electronic medical records from June 1st, 2008 to February 24th, 2016, with approval by the Institutional Review Board at Boston Children Hospital, and identified participants aged under 10 years old (YO) with SNHL according to audiometric tests and otolaryngologic examinations as in our previous study (Shiohama et al., 2019a). The degree of SNHL was determined as mild to moderate (M-M, 26–55 dB HL) and moderately severe to profound (M-P, over 56 dB HL) according to the average of hearing thresholds at 500, 1,000, and 2,000 Hz for pure tone tests of their better ear or sound-field visual reinforcement audiometry tests (Yoshinaga-Itano et al., 2017). We excluded patients with congenital disorders (e.g., Down syndrome, CHARGE syndrome, and other chromosomal abnormalities), perinatal brain damage (hypoxic ischemic encephalopathy and infarction), and premature birth (<37 weeks gestation). The gender- and age-matched neurotypical controls (NC) were selected from our in-house database composed of electronic records of healthy participants without neurological disorders, neuropsychological disorders, or epilepsy (Levman et al., 2017).

2.2 | Acquisition and processing for diffusion MRI tractography

All participants were imaged with clinical 3T MRI scanners (MAGNETOM Skyra, Siemens Medical Systems, Erlangen, Germany) at Boston Children's Hospital. DICOM files of diffusion-weighted MRI were accessed through

the Children's Research and Integration System (Pienaar et al., 2015). Thirty diffusion-weighted measurements (b = 1,000 s/mm^2) and 1 to 10 non-diffusion-weighted measurements (b = 0 s/mm^2) were acquired (repetition time [TR] 4300–12,929 ms; echo time [TE] 88–94 ms; voxel size 1.72 × 1.72 × 2.0 mm; matrix size 128 × 128; flip angle 90° with a head coil). Images with motion artifacts were excluded based on visual assessment (motion correction software was not used). Eighteen diffusion MR images were obtained from 18 participants with SNHL aged under 10 YO. High-angular resolution diffusion imaging (HARDI) (Tuch et al., 2002) was used to reconstruct fibers with Diffusion Toolkit (http;//trackvis.org), using the fiber assignment by continuous tracking (FACT) algorithm (Mori et al., 1999). We did not use an FA threshold to terminate tractography (e.g., Takahashi et al., 2012), but instead used a brain mask to perform tractography within the brain. Callosal pathways (CP) and six associational cortico-cortical fibers (arcuate fasciculus [AF], inferior longitudinal fasciculus [ILF], inferior fronto-occipital fasciculus [IFOF], uncinate fasciculus [UF], cingulum fasciculus [CF], and fornix [Fx]) in both hemispheres were identified and visualized using TrackVis (http;//trackvis.org), as in previous analyses (Cohen et al., 2016; Shiohama et al., 2019b, 2020; Takahashi et al., 2012; Xu et al., 2014).

Anatomic and tractography atlases (Catani & Thiebaut de Schotten, 2008; Mori & Tournier, 2013; Thiebaut de Schotten et al., 2011) were used to guide regions of interest (ROI) placements on non-diffusion-weighted (b0) images and color FA maps in order to delineate the fibers of interest. Two neuroscientists (T.S. and E.T.) identified all tracts through manual ROI placement and assessed resulting courses of fibers in the same way as explained in our past publications (e.g., Cohen et al., 2016; Re et al., 2016). For the AF, CF and Fx fibers, several ROIs were placed along the white matter regions for each fiber shown in the atlases. For the CP, an ROI was drawn in the corpus callosum in a median sagittal plane. For the ILF, IFOF, and UF fibers, two sphere ROIs were used for each region in their pathways: anterior temporal and occipital regions for the ILF, inferior frontal and occipital regions for the IFOF, and inferior frontal and anterior temporal regions for the UF. These ROIs were used as starting and stopping ROIs. When we did not identify any fibers between the starting/stopping ROIs, the distance between the two ROIs were gradually reduced until we found a part of the fibers. Excess erroneous fibers due to the large size of the ROIs were manually excluded using additional sphere ROIs. The size of all ROIs were carefully optimized to exclude other white matter fibers by changing the size and location several times. The color-coding of fibers will be based on a standard red-green-blue (RGB) code, applied to the vector between the endpoints of each fiber (red for right-left, blue for dorsal-ventral, and green for anterior-posterior). The volume, length, FA, and apparent diffusion coefficient (ADC) of each identified pathway were calculated and compared with NC participants.

2.3 | Statistical analysis

Each fiber pathway measurement in SNHL and NC participants, a univariate General Linear model ($p < .05$) were constructed to evaluate the effects of binary or continuous covariates (age and gender). Using statistical function in

TABLE 1 The background of SNHL and NC participants

HARDI tractography study (AF, UF, CF, Fx, and CP)	**SNHL (N = 17)**	**NC (N = 17)**
Male (N [%])	11/17 [65%]	11/17 [65%]
Age of years (mean [SD])[a]	3.8 [2.2]	3.7 [2.4]
Male[b]	3.9 [2.5]	3.9 [2.4]
Female[c]	3.5 [1.3]	3.5 [2.3]
Degree of SNHL (N [%])	M-M 12/17 [71%], M-P 5/17 [29%]	
HARDI tractography study (ILF and IFOF)	**SNHL (N = 14)**	**NC (N = 14)**
Male (N [%])	9/14 [64%]	9/14 [64%]
Age of years (mean [SD])[d]	3.9 [2.4]	3.8 [2.6]
Male[e]	4.1 [2.8]	4.1 [2.6]
Female[f]	3.6 [1.4]	3.2 [2.4]
Degree of SNHL (N [%])	M-M 12/14 [86%], M-P 2/14 [14%]	

Notes: The age of months showed no statistically significant difference between two groups.

Abbreviations: AF, arcuate fasciculus; CF, cingulum fasciculus; CP, callosal pathway; Fx, fornix; HARDI, High-angular resolution diffusion magnetic resonance imaging; IFOF, inferior fronto-occipital fasciculus; ILF, inferior longitudinal fasciculus; M-M, Mild to moderate; M-P, Moderately severe to profound; NC, Neurotypical control; *SD*, Standard deviation; SNHL, Sensorineural hearing loss; UF, uncinate fasciculus.

[a]T(32)=0.0073, p = .994; [b]T(20)=0.016, p = .987; [c]T(8) = −0.014, p = .989; [d]T(26)= 0.125, p = .902; [e]T(16)=0, p = 1; [f]T(6) = 0.243, p = .816.

Excel (Microsoft Corporation, WA) formula, critical values from the F-distribution calculation were determined to be F.INV.RT (0.05, 4, 29) = 2.70 and F.INV.RT (0.05, 1,29) = 4.18 for the corrected model and each covariate, respectively. Cohen's $d = 0.8$ was recognized as a large effect size (Cohen, 1992). IBM SPSS Statistics version 19 (IBM Corp. Armonk, NY) was used for the statistical analysis.

3 | RESULTS

3.1 | Patient characteristics

We collected 17 MRI data sets from 17 participants with SNHL and compared them to those of NC after excluding one MRI data set with poor quality that could not been processed through the software used (see Experimental Procedures).

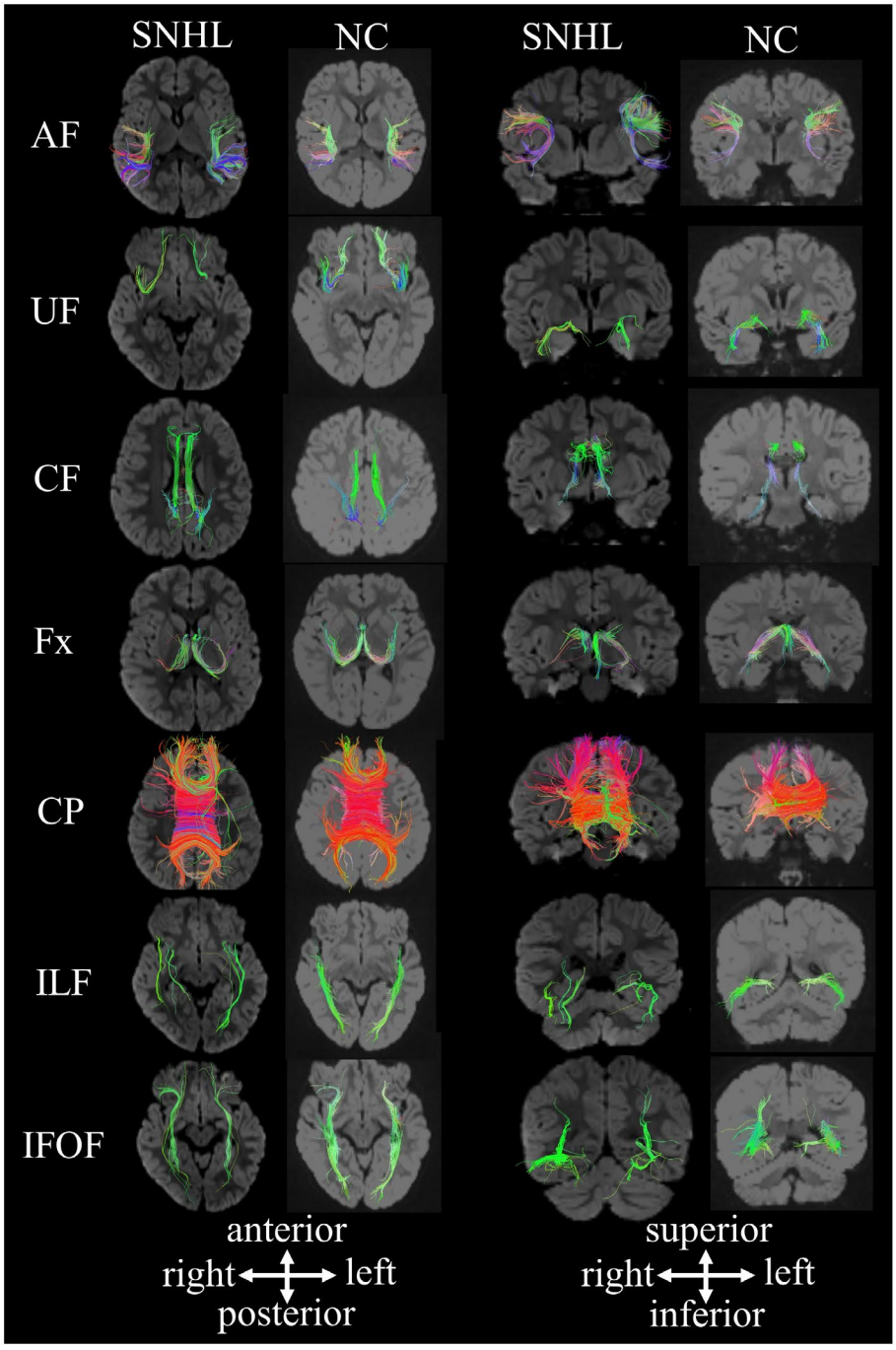

FIGURE 1 Ventral and front views of high-angular resolution diffusion MR imaging tractography of a 2.2-year-old girl with sensorineural hearing loss (SNHL) and a 2.5-year-old neurotypical girl (NC). The density of uncinate fasciculus (UF), inferior longitudinal fasciculus (ILF), and inferior fronto-occipital fasciculus (IFOF) fibers in SNHL were visually lower compared to NC. AF, arcuate fasciculus; CF, cingulum fasciculus; CP, callosal pathways; DTI, diffusion tensor imaging; Fx, fornix; IFOF, inferior fronto-occipital fasciculus; ILF, inferior longitudinal fasciculus; NC, neurotypical control; SNHL, sensorineural hearing loss; UF, uncinate fasciculus [Colour figure can be viewed at wileyonlinelibrary.com]

TABLE 2 HARDI tractography (AF, UF, CF, Fx, and CP) of SNHL and NC participants

Measurements	SNHL ($N = 17$) Mean [*SD*]	NC ($N = 17$) Mean [*SD*]	The rate of SNHL/NC	Cohen's *d*
Volume (ml)				
AF, left	12.3 [4.6]	14.4 [5.2]	0.85	0.43
AF, right	11.4 [3.1]	15.2 [6.0]	0.75	0.79
UF, left	3.1 [1.5]	5.7 [0.9]	0.53	2.18
UF, right	2.8 [1.2]	5.9 [1.4]	0.48	2.38
CF, left	6.0 [1.4]	6.8 [1.8]	0.88	1.30
CF, right	5.5 [1.4]	6.3 [1.5]	0.87	1.13
Fx, left	4.0 [1.2]	6.2 [1.9]	0.65	1.38
Fx, right	4.0 [1.7]	6.0 [2.1]	0.68	1.02
CP	83.7 [21.4]	97.6 [37.6]	0.86	0.45
Lengths (mm)				
AF, left	47.8 [14.2]	43.9 [11.0]	1.09	0.31
AF, right	45.7 [12.6]	41.8 [8.2]	1.09	0.36
UF, left	54.5 [16.5]	39.0 [11.2]	1.40	1.10
UF, right	66.0 [18.0]	41.7 [11.6]	1.58	1.61
CF, left	29.8 [12.8]	39.8 [10.4]	0.75	0.03
CF, right	24.8 [8.6]	36.2 [7.8]	0.69	0.88
Fx, left	50.9 [17.2]	34.1 [7.5]	1.49	1.27
Fx, right	35.7 [14.6]	31.9 [8.3]	1.12	0.32
CP	69.7 [13.3]	63.8 [13.0]	1.09	0.46
FA				
AF, left	0.42 [0.05]	0.42 [0.07]	1.01	0.04
AF, right	0.42 [0.04]	0.42 [0.06]	0.99	0.05
UF, left	0.40 [0.05]	0.39 [0.07]	1.02	0.14
UF, right	0.40 [0.04]	0.39 [0.08]	1.02	0.15
CF, left	0.43 [0.07]	0.43 [0.07]	1.00	0.18
CF, right	0.41 [0.05]	0.42 [0.07]	0.98	0.22
Fx, left	0.36 [0.06]	0.38 [0.08]	0.96	0.22
Fx, right	0.33 [0.04]	0.37 [0.09]	0.89	0.59
CP	0.56 [0.03]	0.52 [0.07]	1.07	0.66
ADC ($mm^2/s \times 10^{-4}$)				
AF, left	8.9 [1.2]	7.5 [1.7]	1.19	0.95
AF, right	8.8 [0.6]	7.5 [1.7]	1.17	0.99
UF, left	9.1 [0.6]	7.9 [1.5]	1.15	1.02
UF, right	9.3 [0.5]	7.9 [1.5]	1.17	1.15
CF, left	9.2 [0.7]	7.7 [1.6]	1.18	1.18
CF, right	9.2 [0.6]	7.7 [1.5]	1.20	1.31
Fx, left	12.8 [1.7]	9.5 [2.1]	1.35	1.75
Fx, right	13.1 [2.1]	9.7 [2.3]	1.36	1.59
CP	9.5 [0.8]	7.69 [1.8]	1.23	1.27

Abbreviations: ADC, apparent diffusion coefficient; AF, arcuate fasciculus; CF, cingulum fasciculus; CP, callosal pathway; FA, fractional anisotropy; Fx, fornix; HARDI, High-angular resolution diffusion magnetic resonance imaging; NC, Neurotypical control; *SD*, Standard deviation; SNHL, Sensorineural hearing loss; UF, uncinate fasciculus.

Gender and age at MRI scans in SNHL participants were matched to those of NC (ratio of males, SNHL 11/17, NC 11/17; age at scans, SNHL mean 3.8 YO [standard deviation 2.2], NC 3.7 [2.4], [T (32) = 0.0073, $p = .994$]) (Table 1).

3.2 | HARDI tractography

We identified the AF, UF, CF, Fx, CP, ILF, and IFOF in SNHL and NC participants using HARDI tractography (Figure 1). Among the 17 participants with SNHL, the left ILF and left IFOF in participant (2.9 YO boy), right ILF in participant (3.3 YO boy), and right IFOF in three participants (2.9 YO boy, 3.3 YO boy, and 3.2 YO girl) were partly undetected. Therefore, the measurements of the ILF and IFOF were statistically compared between only 14 participants in each group who had full lengths of the ILF and IFOF detected (Table 1).

The ratio of volumes, length, FA, and ADC values in SNHL to NC ranged 0.43–0.86, 0.75–1.66, 0.89–1.07, and 1.14–1.36, respectively (Tables 2 and 3).

The presence of SNHL was an independent significant factor in the decreased volumes of the bilateral UF, Fx, ILF, and IFOF, the increased length of the bilateral UF, ILF, and IFOF, and left Fx, the decreased length of the bilateral CF, and increased ADC values in the bilateral AF, UF, CF, Fx, ILF, and IFOF, and CP. FA value showed no statistically significant differences (Tables 4 and 5).

4 | DISCUSSION

We focused on long association fibers in SNHL using diffusion MRI tractography metrics and, in multiple fibers, found decreased volumes, increased lengths, and higher ADC values without difference of FA values in SNHL compared to NC.

4.1 | HARDI tractography

In this study, we utilized HARDI instead of traditional diffusion tensor imaging (DTI), due to HARDI's potential advantage for detecting fibers in immature brains, which posse a surplus of unmyelinated or hardly myelinated fibers (e.g., Frank, 2002; Takahashi et al., 2014; Wilkinson et al., 2017). HARDI theoretically enables better differentiation within a voxel by utilizing information about water diffusivity from many more directions than DTI (Tuch et al., 2002). The white matter fibers in SNHL have been analyzed in only a few studies using tract-based spatial statistics (TBSS), which showed lower FA values of the bilateral AF, UF, ILF, and IFOF in profound SNHL patients aged below

TABLE 3 HARDI tractography (ILF and IFOF) of SNHL and NC participants

Measurements	SNHL ($N = 14$) Mean [*SD*]	NC ($N = 14$) Mean [*SD*]	The rate of SNHL/NC	Cohen's *d*
Volume (ml)				
ILF, left	4.8 [2.3]	7.9 [1.6]	0.60	1.58
ILF, right	3.6 [1.2]	7.9 [1.8]	0.45	2.84
IFOF, left	5.7 [2.3]	12.2 [2.8]	0.47	2.55
IFOF, right	5.5 [2.0]	12.8 [3.4]	0.43	2.63
Lengths (mm)				
ILF, left	67.0 [10.8]	50.2 [6.3]	1.34	1.91
ILF, right	66.4 [14.5]	43.2 [6.1]	1.54	2.09
IFOF, left	98.2 [20.5]	59.1 [13.4]	1.66	2.26
IFOF, right	96.6 [23.3]	60.6 [9.4]	1.59	2.02
FA				
ILF, left	0.45 [0.06]	0.48 [0.07]	0.95	0.38
ILF, right	0.44 [0.06]	0.47 [0.07]	0.93	0.48
IFOF, left	0.48 [0.05]	0.48 [0.06]	0.99	0.09
IFOF, right	0.47 [0.04]	0.47 [0.06]	1.00	0.04
ADC ($mm^2/s \times 10^{-4}$)				
ILF, left	9.6 [0.9]	8.2 [1.8]	1.16	0.93
ILF, right	9.6 [0.9]	8.3 [1.9]	1.16	0.87
IFOF, left	9.2 [0.9]	8.0 [1.7]	1.15	0.89
IFOF, right	9.2 [0.8]	8.0 [1.7]	1.14	0.87

Abbreviations: ADC, apparent diffusion coefficient; FA, fractional anisotropy; HARDI, High-angular resolution diffusion magnetic resonance imaging; IFOF, inferior fronto-occipital fasciculus; ILF, inferior longitudinal fasciculus; NC, Neurotypical control; *SD*, Standard deviation; SNHL, Sensorineural hearing loss.

TABLE 4 The effects of covariates on HARDI tractography measurements (AF, UF, CF, Fx, and CP); Univariate general linear model

Measurements	Adjusted R^2	Corrected model	SNHL	Gender	Age
Volume					
AF, left	0.077	$F = 0.41, p = .80$	$F = 1.16, p = .29$	$F = 0.07, p = .80$	$F = 0.09, p = .77$
AF, right	0.080	$F = 1.72, p = .17$	$F = 3.55, p = .07$	$F = 0.06, p = .82$	$F = 0.71, p = .40$
UF, left	0.508	**$F = 9.52, p = 4.8 \times 10^{-5}$**	**$F = 32.3, p = 3.8 \times 10^{-6}$**	$F = 0.0016, p = .97$	$F = 0.29, p = .59$
UF, right	0.591	**$F = 12.9, p = 3.7 \times 10^{-6}$**	**$F = 44.0, p = 2.8 \times 10^{-7}$**	$F = 0.31, p = .58$	$F = 2.97, p = .095$
CF, left	0.016	$F = 0.87, p = .49$	$F = 2.7, p = .11$	$F = 0.15, p = .70$	$F = 0.64, p = .43$
CF, right	0.004	$F = 0.96, p = .44$	$F = 3.0, p = .09$	$F = 0.01, p = .91$	$F = 0.83, p = .37$
Fx, left	0.278	**$F = 4.2, p = 8.6 \times 10^{-3}$**	**$F = 15.3, p = 5.1 \times 10^{-4}$**	$F = 0.068, p = .80$	$F = 1.03, p = .32$
Fx, right	0.210	**$F = 3.2, p = .027$**	**$F = 9.0, p = 5.5 \times 10^{-3}$**	$F = 2.8, p = .11$	$F = 0.61, p = .44$
CP	0.261	**$F = 3.9, p = .011$**	$F = 2.9, p = .10$	**$F = 4.5, p = .043$**	**$F = 9.1, p = 5.3 \times 10^{-3}$**
Lengths					
AF, left	0.071	$F = 0.45, p = .77$	$F = 0.64, p = .43$	$F = 4.3 \times 10^{-3}, p = .95$	$F = 1.03, p = .32$
AF, right	0.034	$F = 0.73, p = .58$	$F = 1.7, p = .20$	$F = 0.58, p = .45$	$F = 0.13, p = .72$
UF, left	0.199	**$F = 3.1, p = .03$**	**$F = 11.1, p = 2.4 \times 10^{-3}$**	$F = 0.95, p = .34$	$F = 0.22, p = .64$
UF, right	0.366	**$F = 5.8, p = 1.5 \times 10^{-3}$**	**$F = 19.2, p = 1.4 \times 10^{-4}$**	$F = 1.16, p = .29$	$F = 0.77, p = .39$
CF, left	0.206	**$F = 3.1, p = .029$**	**$F = 6.2, p = .019$**	$F = 0.70, p = .41$	**$F = 5.3, p = .03$**
CF, right	0.310	**$F = 4.7, p = 4.8 \times 10^{-3}$**	**$F = 13.7, p = 8.8 \times 10^{-4}$**	$F = 2.7 \times 10^{-3}, p = .96$	$F = 1.9, p = .18$
Fx, left	0.278	**$F = 4.2, p = 8.6 \times 10^{-3}$**	**$F = 9.5, p = 4.5 \times 10^{-3}$**	$F = 0.51, p = .48$	$F = 0.14, p = .71$
Fx, right	0.016	$F = 0.87, p = .49$	$F = 0.38, p = .54$	$F = 0.18, p = .67$	$F = 1.72, p = .20$
CP	0.158	$F = 2.6, p = .06$	$F = 2.8, p = .10$	$F = 2.1, p = .15$	**$F = 5.2, p = .03$**
FA					
AF, left	0.061	$F = 1.5, p = .22$	$F = 0.02, p = .88$	$F = 1.9, p = .18$	$F = 3.8, p = .06$
AF, right	0.000	$F = 1.0, p = .42$	$F = 0.14, p = .71$	$F = 1.2, p = .28$	$F = 2.3, p = .14$
UF, left	0.076	$F = 0.42, p = .79$	$F = 0.2, p = .66$	$F = 1.1, p = .29$	$F = 0.24, p = .63$
UF, right	0.067	$F = 0.48, p = .75$	$F = 0.1, p = .75$	$F = 1.5, p = .24$	$F = 0.15, p = .70$
CF, left	0.082	$F = 0.38, p = .82$	$F = 0.01, p = .92$	$F = 0.17, p = .68$	$F = 1.3, p = .26$
CF, right	0.094	$F = 0.29, p = .88$	$F = 0.31, p = .58$	$F = 0.34, p = .57$	$F = 0.46, p = .50$
Fx, left	0.120	$F = 0.11, p = .98$	$F = 0.34, p = .56$	$F = 2.5 \times 10^{-3}, p = .96$	$F = 0.09, p = .77$
Fx, right	0.026	$F = 0.79, p = .54$	$F = 2.4, p = .13$	$F = 0.18, p = .67$	$F = 0.26, p = .62$
CP	0.020	$F = 1.2, p = .35$	$F = 2.8, p = .10$	$F = 0.30, p = .59$	$F = 0.84, p = .37$
ADC					
AF, left	0.270	**$F = 4.1, p = .01$**	**$F = 9.0, p = 5.4 \times 10^{-3}$**	$F = 3.6, p = .068$	$F = 4.0, p = .054$
AF, right	0.279	**$F = 4.2, p = 8.4 \times 10^{-3}$**	**$F = 10.2, p = 3.4 \times 10^{-3}$**	$F = 2.8, p = .11$	**$F = 4.3, p = .046$**

(Continues)

TABLE 4 (Continued)

Measurements	Adjusted R^2	Corrected model	SNHL	Gender	Age
UF, left	0.256	$\mathbf{F = 3.8, p = .013}$	$\mathbf{F = 10.2, p = 3.4 \times 10^{-3}}$	$F = 2.7, p = .11$	$F = 2.9, p = .099$
UF, right	0.284	$\mathbf{F = 4.3, p = 7.7 \times 10^{-3}}$	$\mathbf{F = 12.8, p = 1.3 \times 10^{-3}}$	$F = 2.2, p = .15$	$F = 2.5, p = .12$
CF, left	0.346	$\mathbf{F = 5.4, p = 2.3 \times 10^{-3}}$	$\mathbf{F = 15.3, p = 5.1 \times 10^{-4}}$	$F = 3.4, p = .074$	$F = 3.1, p = .089$
CF, right	0.353	$\mathbf{F = 5.5, p = 2.0 \times 10^{-3}}$	$\mathbf{F = 16.9, p = 2.9 \times 10^{-4}}$	$F = 2.4, p = .13$	$F = 3.0, p = .093$
Fx, left	0.406	$\mathbf{F = 6.6, p = 6.4 \times 10^{-3}}$	$\mathbf{F = 21.1, p = 7.8 \times 10^{-5}}$	$F = 0.22, p = .65$	$F = 1.05, p = .31$
Fx, right	0.423	$\mathbf{F = 7.1, p = 4.3 \times 10^{-4}}$	$\mathbf{F = 17.1, p = 2.8 \times 10^{-4}}$	$F = 2.8, p = .103$	$F = 0.025, p = .87$
CP	0.370	$\mathbf{F = 5.8, p = 1.4 \times 10^{-3}}$	$\mathbf{F = 15.3, p = 5.1 \times 10^{-4}}$	$F = 4.2, p = .051$	$F = 3.9, p = .057$

Notes: Bold numbers indicate values with a statistical significance. General Linear Model ($p < .05$) was constructed to evaluate of binary or continuous covariates (gender and age). Statistically significant values from the F-distribution calculation were determined to be 2.70 and 4.18 for the corrected model and each covariate, respectively.

Abbreviations: ADC, apparent diffusion coefficient; AF, arcuate fasciculus; CF, cingulum fasciculus; CP, callosal pathway; FA, fractional anisotropy; Fx, fornix; HARDI, High-angular resolution diffusion magnetic resonance imaging; SNHL, Sensorineural hearing loss; UF, uncinate fasciculus.

4 years (Park et al., 2018; Wang, Chen, et al., 2019). In contrast, other measurements (volume, lengths, and ADC values) of long association fibers in SNHL have not been focused on so far. In our study, lower volumes of the bilateral UF, Fx, ILF, and IFOF were observed in children with SNHL. Interestingly, the ILF and IFOF were undetected in three participants with profound SNHL. Although recognizable brain atrophy was not observed in participants in this study, the possibility that these regional changes are affected by partial volume effects, such as gray matter of CSF contamination (Roine et al., 2014) or multiple fiber configurations (Jeurissen et al., 2013; Vos et al., 2011) cannot be completely excluded.

4.2 | Long association fibers and cognitive functions

The long association fibers are involved in language processing (Friederici, 2015; Hickok & Peeppoel, 2007) and other cognitive functions. The AF is a lateral associative bundle, which is directly and indirectly connecting Broca's area (in the inferior frontal cortex), Geschwind's area (in the inferior parietal cortex), and Wernicke's area (in the superior temporal cortex) (Catani et al., 2005; Friederici, 2015). The right AF also participates in visuospatial processing (Doricchi et al., 2008), prosody, and semantic processing (Catani et al., 2007). The UF possibly plays a role in emotion processing (Gaffan & Wilson, 2008; Ross, 2008), memory (Gaffan & Wilson, 2008; Ross, 2008), and language function (Catani & Mesulam, 2008). The CF and Fx are part of the limbic system (Catani et al., 2002; Catani & Thiebaut de Schotten, 2008), related to attention, memory, and emotions (Gaffan & Wilson, 2008; Ross, 2008; Rudrauf et al., 2008). The ILF and IFOF, which mainly connect regions of the fronto-parieto-temporal network, can be considered as a part of the speech processing stream (dual stream model) (Hickok & Poeppel, 2007). The ILF is a ventral associative bundle connecting the occipital and ipsilateral temporal lobes (Catani et al., 2002; Catani & Thiebaut de Schotten, 2008), which potentially governs face recognition (Fox et al., 2008), visual perception (Ffytche, 2008), reading (Epelbaum et al., 2008), and visual memory (Ross, 2008). The IFOF is a ventral associative bundle connecting the ventral occipital lobe and the orbitofrontal cortex (Catani et al., 2002; Catani & Thiebaut de Schotten, 2008), which is potentially linked to reading (Catani & Mesulam, 2008), attention (Doricchi et al., 2008), and visual processing (Fox et al., 2008; Rudrauf et al., 2008).

4.3 | FA and ADC values on HARDI-derived fibers

The FA and ADC values represent the degree of directionality of microstructures and the degree of water diffusivity, respectively. The pattern of increased ADC values with decreased FA values in cerebral white matter has been associated with vasogenic edema (Pasternak et al., 2009), multiple sclerosis (Roosendaal et al., 2009; Vishwas et al., 2013), and the infantile period (Löbel et al., 2009). The pattern of decreased volume and increased ADC values with normal FA values, which was observed in long association fibers in the SNHL group in this study, may indicate the presence of a

low density of cortico-cortical fibers in SNHL, although histopathological observation could not be carried out by our study or other investigators.

4.4 | Impairment of the long association fibers and auditory deprivation

It remains unclear whether these changes in long association fibers in participants with SNHL was purely caused by auditory deprivation during intrauterine and early infantile period. Because we did not assess fetal brain MRI of both groups before the establishment of auditory systems, there is the possibility that another factor such as cerebral hypoxia led to both SNHL and affected long association fibers. However, we excluded patients with congenital disorders, perinatal brain damage, and premature birth by physical examination and MRI qualitative study. Even mild to moderate types of peripheral hypoxic ischemia encephalopathy present subsequent cerebral volume loss (Bano et al., 2017; Bregant et al., 2013), and our SNHL participants showed no significant cerebral volume loss (see our previous report,

TABLE 5 The effects of covariates on HARDI tractography measurements (ILF and IFOF); univariate general linear model

Measurements	Adjusted R^2	Corrected model	SNHL	Gender	Age
Volume					
ILF, left	0.410	$\mathbf{F = 5.7, p = 2.5 \times 10^{-3}}$	$\mathbf{F = 21.8, p = 1.1 \times 10^{-4}}$	$F = 0.03, p = .86$	$F = 0.8, p = .38$
ILF, right	0.650	$\mathbf{F = 13.5, p = 8.3 \times 10^{-6}}$	$\mathbf{F = 45.6, p = 6.9 \times 10^{-7}}$	$F = 0.04, p = .84$	$F = 0.7, p = .41$
IFOF, left	0.619	$\mathbf{F = 12.0, p = 2.1 \times 10^{-5}}$	$\mathbf{F = 45.2, p = 7.5 \times 10^{-7}}$	$F = 0.09, p = .76$	$F = 1.8, p = .20$
IFOF, right	0.758	$\mathbf{F = 22.1, p = 1.3 \times 10^{-7}}$	$\mathbf{F = 63.1, p = 4.8 \times 10^{-8}}$	$F = 0.25, p = .62$	$F = 13.6, p = 1.2 \times 10^{-3}$
Lengths					
ILF, left	0.466	$\mathbf{F = 6.9, p = 8.5 \times 10^{-4}}$	$\mathbf{F = 24.4, p = 5.4 \times 10^{-5}}$	$F = 1.7, p = .20$	$F = 0.3, p = .57$
ILF, right	0.473	$\mathbf{F = 7.1, p = 7.4 \times 10^{-4}}$	$\mathbf{F = 26.2, p = 3.5 \times 10^{-5}}$	$F = 0.51, p = .48$	$F = 0.05, p = .82$
IFOF, left	0.589	$\mathbf{F = 10.7, p = 4.9 \times 10^{-5}}$	$\mathbf{F = 38.6, p = 2.5 \times 10^{-6}}$	$F = 2.3, p = .14$	$F = 1.2, p = .28$
IFOF, right	0.646	$\mathbf{F = 13.3, p = 9.2 \times 10^{-6}}$	$\mathbf{F = 42.4, p = 1.2 \times 10^{-6}}$	$\mathbf{F = 7.5, p = .012}$	$F = 3.7, p = .068$
FA					
ILF, left	0.105	$F = 1.8, p = .16$	$F = 1.6, p = .22$	$F = 0.42, p = .53$	$\mathbf{F = 5.6, p = .026}$
ILF, right	0.059	$F = 1.4, p = .26$	$F = 2.6, p = .12$	$F = 0.01, p = .93$	$F = 2.7, p = .11$
IFOF, left	0.082	$F = 0.5, p = .74$	$F = 0.06, p = .81$	$F = 0.03, p = .86$	$F = 1.9, p = .18$
IFOF, right	0.033	$F = 0.8, p = .55$	$F = 0.01, p = .91$	$F = 0.79, p = .38$	$F = 2.7, p = .12$
ADC					
ILF, left	0.268	$\mathbf{F = 3.5, p = .023}$	$\mathbf{F = 8.3, p = 8.6 \times 10^{-3}}$	$F = 2.9, p = .104$	$F = 3.9, p = .062$
ILF, right	0.285	$\mathbf{F = 3.7, p = .018}$	$\mathbf{F = 7.7, p = .011}$	$F = 3.2, p = .08$	$\mathbf{F = 5.1, p = .034}$
IFOF, left	0.226	$\mathbf{F = 3.0, p = .041}$	$\mathbf{F = 6.7, p = .016}$	$F = 3.6, p = .069$	$F = 2.5, p = .13$
IFOF, right	0.261	$\mathbf{F = 3.4, p = .026}$	$\mathbf{F = 7.2, p = .013}$	$F = 3.2, p = .089$	$\mathbf{F = 4.3, p = .048}$

Notes: Bold numbers indicate values with a statistical significance. General Linear Model ($p < .05$) was constructed to evaluate of binary or continuous covariates (gender and age). Statistically significant values from the F-distribution calculation were determined to be 2.70 and 4.18 for the corrected model and each covariate, respectively.

Abbreviations: ADC, apparent diffusion coefficient; FA, fractional anisotropy; HARDI, High-angular resolution diffusion magnetic resonance imaging; IFOF, inferior fronto-occipital fasciculus; ILF, inferior longitudinal fasciculus; SNHL, Sensorineural hearing loss.

Shiohama et al., 2019a), suggesting that the SNHL participants in our study had no profound perinatal brain damages.

Our previous study of CHARGE syndrome showed decreased volumes, increased lengths, and increased ADC without difference of FA values in multiple long association fibers, as compared to NC (Shiohama et al., 2019b). Interestingly, although patients with CHARGE syndrome were clinically excluded from participants in the current study, the pattern of measurements for HARDI-derived long association fibers in SNHL was similar to those in CHARGE syndrome (Shiohama et al., 2019b). Since hearing loss due to cranial nerve aphasia and/ or semicircular canal hypoplasia is often observed in patients with CHARGE syndrome (Hoch et al., 2017), the differences between CHARGE syndrome and NC groups may partly depend on the presence of SNHL in CHARGE syndrome.

4.5 | Limitations

Some limitations exist in this study. First, the possible presence of selection bias (health-care access bias) could not be excluded because this study was retrospectively carried out in a single medical facility. Second, although we excluded patients with congenital disorders, perinatal brain damage, and premature birth to exclude major confounders, our medical records did not include the information regarding the developmental quotient, cognitive function except for auditory function, and handedness. Future studies are necessary to test associations between these factors and affected HARDI-derived fibers in SNHL. Third, MRI acquisition was carried out using clinical scans across many years, therefore, diffusion parameters in our study sometimes varied, although routine clinical scans usually use preset parameters to quickly diagnose. Finally, the proportion of degree of hearing loss in this study (M-M 71%, M-P 29%) did not completely meet the proportions in a previous cross-section study (M-M 57%, M-P 43%) (Yoshinaga-Itano et al., 2017), and studies using TBSS (profound 100%) (Park et al., 2018; Wang, Liang, et al., 2019; Wang, Chen, et al., 2019). The difference of enrollment criteria potentially affects universality of analysis results. Another limitation is that we could not account intracerebral volume as covariates, because our data set did not include T1-weighted images of the neurotypical controls. Therefore, we could not completely exclude the possibility of whole brain volume to affect the measurements of the long association fibers.

5 | CONCLUSION

Our quantitative study of HARDI-derived long association fibers in participants with SHNL showed increased length, decreased volume, and higher ADC in multiple fibers, compared to those of NC. The impairment of long association fibers in SNHL may partly be related to the association of cognitive dysfunction with SNHL.

ACKNOWLEDGEMENTS

We thank Elizabeth Ethier for proofreading this paper. This research project was supported by National Institutes of Health (R01HD078561, R21MH118739, R21HD098606, and R03NS101372) to E.T., Natural Science and Engineering Research Council of Canada's Canada Research Chair grant (231266), a Canada Foundation for Innovation and Nova Scotia Research and Innovation Trust infrastructure grant (R0176004), and a St. Francis Xavier University research startup grant (R0168020) to J.L.

CONFLICT OF INTEREST

T.S., B.C., J. L., and E. T. declare relevant no conflicts of interest.

ETHICAL APPROVAL

All procedures performed in the studies involving human participants were in accordance with the ethical standards of the institutional and/or national research committee and with the 1964 Helsinki Declaration and its later amendments or similar ethical standards.

INFORMED CONSENT

For this type of study, formal consent is not required.

DATA AVAILABILITY STATEMENT

The data that support the findings of this study are available from the corresponding author upon reasonable request.

AUTHOR CONTRIBUTIONS

T.S. was responsible for study design. J.L. assembled data. T.S., B.C., and E.T. analyzed data. T.S., J.L., and E.T. wrote/ edited the manuscript.

ORCID

Tadashi Shiohama https://orcid.org/0000-0003-0076-5882

REFERENCES

Bano, S., Chaudhary, V., & Garga, U. C. (2017). Neonatal hypoxic-ischemic encephalopathy: A radiological review. *Journal of Pediatric Neurosciences*, *12*, 1–6. https://doi.org/10.4103/1817-1745.205646

Berger, C., Kühne, D., Scheper, V., & Kral, A. (2017). Congenital deafness affects deep layers in primary and secondary auditory cortex. *The Journal of Comparative Neurology*, *525*, 3110–3125. https://doi.org/10.1002/cne.24267

Bergeson, T. R., Houston, D. M., & Miyamoto, R. T. (2010). Effects of congenital hearing loss and cochlear implantation on audiovisual speech perception in infants and children. *Restorative*

Neurology and Neuroscience, *28*, 157–165. https://doi.org/10.3233/RNN-2010-0522

Bregant, T., Rados, M., Vasung, L., Derganc, M., Evans, A. C., Neubauer, D., & Kostovic, I. (2013). Region-specific reduction in brain volume in young adults with perinatal hypoxic-ischaemic encephalopathy. *European Journal of Paediatric Neurology*, *17*, 608–614. https://doi.org/10.1016/j.ejpn.2013.05.005

Buckley, K. A., & Tobey, E. A. (2011). Cross-modal plasticity and speech perception in pre- and postlingually deaf cochlear implant users. *Ear and Hearing*, *32*, 2–15. https://doi.org/10.1097/AUD.0b013e3181e8534c

Catani, M., Allin, M. P., Husain, M., Pugliese, L., Mesulam, M. M., Murray, R. M., & Jones, D. K. (2007). Symmetries in human brain language pathways correlate with verbal recall. *Proceedings of the National Academy of Sciences*, *104*, 17163–17168. https://doi.org/10.1073/pnas.0702116104

Catani, M., Howard, R. J., Pajevic, S., & Jones, D. K. (2002). Virtual in vivo interactive dissection of white matter fasciculi in the human brain. *NeuroImage*, *171*, 77–94. https://doi.org/10.1006/nimg.2002.1136

Catani, M., Jones, D. K., & ffytche, D. H. (2005). Perisylvian language networks of the human brain. *Annals of Neurology*, *57*, 8–16. https://doi.org/10.1002/ana.20319

Catani, M., & Mesulam, M. (2008). The arcuate fasciculus and the disconnection theme in language and aphasia: History and current state. *Cortex*, *44*, 953–961. https://doi.org/10.1016/j.cortex.2008.04.002

Catani, M., & Thiebaut de Schotten, M. (2008). A diffusion tensor imaging tractography atlas for virtual in vivo dissections. *Cortex*, *44*, 1105–1132. https://doi.org/10.1016/j.cortex.2008.05.004

Chang, Y., Lee, H. R., Paik, J. S., Lee, K. Y., & Lee, S. H. (2012). Voxel-wise analysis of diffusion tensor imaging for clinical outcome of cochlear implantation: Retrospective study. *Clinical and Experimental Otorhinolaryngology*, *5*, S37–42. https://doi.org/10.3342/ceo.2012.5.S1.S37

Cohen, A. H., Wang, R., Wilkinson, M., MacDonald, P., Lim, A. R., & Takahashi, E. (2016). Development of human white matter fiber pathways: From newborn to adult ages. *International Journal of Developmental Neuroscience*, *50*, 26–38. https://doi.org/10.1016/j.ijdevneu.2016.02.002

Cohen, J. (1992). A power primer. *Psychological Bulletin*, *112*, 155–159. https://doi.org/10.1037/0033-2909.112.1.155

Doricchi, F., Thiebaut de Schotten, M., Tomaiuolo, F., & Bartolomeo, P. (2008). White matter (dis)connections and gray matter (dys)functions in visual neglect: Gaining insights into the brain networks of spatial awareness. *Cortex*, *44*, 983–995. https://doi.org/10.1016/j.cortex.2008.03.006

Dye, M. W. (2014). Temporal entrainment of visual attention in children: Effects of age and deafness. *Vision Research*, *105*, 29–36.

Dye, M. W., & Hauser, P. C. (2014). Sustained attention, selective attention and cognitive control in deaf and hearing children. *Hearing Research*, *309*, 94–102.

Epelbaum, S., Pinel, P., Gaillard, R., Delmaire, C., Perrin, M., Dupont, S., Dehaene, S., & Cohen, L. (2008). Pure alexia as a disconnection syndrome: New diffusion imaging evidence for an old concept. *Cortex*, *44*, 962–974. https://doi.org/10.1016/j.cortex.2008.05.003

Ffytche, D. H. (2008). The hodology of hallucinations. *Cortex*, *44*, 1067–1083. https://doi.org/10.1016/j.cortex.2008.04.005

Filley, C. M., & Fields, R. D. (2016). White matter and cognition: Making the connection. *Journal of Neurophysiology*, *116*, 2093–2104.

Fox, C. J., Iaria, G., & Barton, J. J. (2008). Disconnection in prosopagnosia and face processing. *Cortex*, *44*, 996–1009.

Frank, L. R. (2002). Characterization of anisotropy in high angular resolution diffusion-weighted MRI. *Magnetic Resonance in Medicine*, *47*, 1083–1099.

Friederici, A. D. (2015). White-matter pathways for speech and language processing. *Handbook of Clinical Neurology*, *129*, 177–186.

Gaffan, D., & Wilson, C. R. (2008). Medial temporal and prefrontal function: Recent behavioural disconnection studies in the macaque monkey. *Cortex*, *44*, 928–935. https://doi.org/10.1016/j.cortex.2008.03.005

Garel, C., Chantrel, E., Elmaleh, M., Brisse, H., & Sebag, G. (2003). Fetal MRI: Normal gestational landmarks for cerebral biometry, gyration and myelination. *Childs Nervous System*, *19*, 422–425. https://doi.org/10.1007/s00381-003-0767-4

Hickok, G., & Poeppel, D. (2007). The cortical organization of speech processing. *Nature Reviews Neuroscience*, *8*, 393–402. https://doi.org/10.1038/nrn2113

Hoch, M. J., Patel, S. H., Jethanamest, D., Win, W., Fatterpekar, G. M., Roland, J. T., & Hagiwara, M. (2017). Head and neck MRI findings in CHARGE syndrome. *American Journal of Neuroradiology*, *38*, 2357–2363. https://doi.org/10.3174/ajnr.A5297

Hribar, M., Suput, D., Carvalho, A. A., Battelino, S., & Vovk, A. (2014). Structural alterations of brain grey and white matter in early deaf adults. *Hearing Research*, *318*, 1–10. https://doi.org/10.1016/j.heares.2014.09.008

Jeurissen, B., Leemans, A., Tournier, J. D., Jones, D. K., & Sijbers, J. (2013). Investigating the prevalence of complex fiber configurations in white matter tissue with diffusion magnetic resonance imaging. *Human Brain Mapping*, *34*, 2747–2766.

Jiang, M., Wen, Z., Long, L., Wong, C. W., Ye, N., Zee, C., & Chen, B. T. (2019). Assessing cerebral white matter microstructure in children with congenital sensorineural hearing loss: A tract-based spatial statistics study. *Frontiers in Neuroscience*, *13*, 597. https://doi.org/10.3389/fnins.2019.00597

Kral, A. (2013). Auditory critical periods: A review from system's perspective. *Neuroscience*, *247*, 117–133. https://doi.org/10.1016/j.neuroscience.2013.05.021

Kral, A., Kronenberger, W. G., Pisoni, D. B., & O'Donoghue, G. M. (2016). Neurocognitive factors in sensory restoration of early deafness: A connectome model. *The Lancet Neurology*, *15*, 610–621. https://doi.org/10.1016/S1474-4422(16)00034-X

Kral, A., & O'Donoghue, G. M. (2010). Profound deafness in childhood. *New England Journal of Medicine*, *363*, 1438–1450. https://doi.org/10.1056/NEJMra0911225

Kronenberger, W. G., Beer, J., Castellanos, I., Pisoni, D. B., & Miyamoto, R. T. (2014). Neurocognitive risk in children with cochlear implants. *JAMA Otolaryngology–head & Neck Surgery*, *140*, 608–615. https://doi.org/10.1001/jamaoto.2014.757

Levman, J., MacDonald, P., Lim, A. R., Forgeron, C., & Takahashi, E. (2017). A pediatric structural MRI analysis of healthy brain development from newborns to young adults. *Human Brain Mapping*, *38*, 5931–5942. https://doi.org/10.1002/hbm.23799

Li, J., Li, W., Xian, J., Li, Y., Liu, Z., Liu, S., Wang, X., Wang, Z., & He, H. (2012). Cortical thickness analysis and optimized voxel-based morphometry in children and adolescents with prelingually profound sensorineural hearing loss. *Brain Research*, *1430*, 35–42.

Löbel, U., Sedlacik, J., Güllmar, D., Kaiser, W. A., Reichenbach, J. R., & Mentzel, H. J. (2009). Diffusion tensor imaging: The normal

evolution of ADC, RA, FA, and eigenvalues studied in multiple anatomical regions of the brain. *Neuroradiology*, *51*, 253–263. https://doi.org/10.1007/s00234-008-0488-1

Lomber, S. G., Meredith, M. A., & Kral, A. (2010). Cross-modal plasticity in specific auditory cortices underlies visual compensations in the deaf. *Nature Neuroscience*, *13*, 1421–1427. https://doi.org/10.1038/nn.2653

Martines, F., Martines, E., Mucia, M., Sciacca, V., & Salvago, P. (2013). Prelingual sensorineural hearing loss and infants at risk: Western Sicily report. *International Journal of Pediatric Otorhinolaryngology*, *77*, 513–518. https://doi.org/10.1016/j.ijporl.2012.12.023

McCaskey, U., von Aster, M., O'Gorman, R., & Kucian, K. (2020). Persistent differences in brain structure in developmental dyscalculia: A longitudinal morphometry study. *Frontiers in Human Neuroscience*, *14*, 272.

Mori, S., Crain, B. J., Chacko, V. P., & Van Zijl, P. C. M. (1999). Three-dimensional tracking of axonal projections in the brain by magnetic resonance imaging. *Annals of Neurology*, *45*, 265–269. https://doi.org/10.1002/1531-8249(199902)45:2<265:AID-ANA21>3.0.CO;2-3

Mori, S., & Tournier, J. D. (2013). *Introduction to diffusion tensor imaging* (1st. ed., p. 140). Academic Press.

Oostra, K. M., Van Bladel, A., Vanhoonacker, A. C., & Vingerhoets, G. (2016). Damage to fronto-parietal networks impairs motor imagery ability after stroke: A voxel-based lesion symptom mapping study. *Frontiers in Behavioural Neurosciences*, *10*, 5.

Park, K. H., Chung, W. H., Kwon, H., & Lee, J. M. (2018). Evaluation of cerebral white matter in prelingually deaf children using diffusion tensor imaging. *BioMed Research International*, *2018*, 1–7. https://doi.org/10.1155/2018/6795397

Pasternak, O., Sochen, N., Gur, Y., Intrator, N., & Assaf, Y. (2009). Free water elimination and mapping from diffusion MRI. *Magnetic Resonance in Medicine*, *62*, 717–730. https://doi.org/10.1002/mrm.22055

Petro, L. S., Paton, A. T., & Muckli, L. (2017). Contextual modulation of primary visual cortex by auditory signals. *Philosophical Transactions of the Royal Society of London. Series B, Biological Sciences*, *372*, 20160104. https://doi.org/10.1098/rstb.2016.0104

Pienaar, R., Rannou, N., Bernal, J., Hahn, D., & Grant, P. E. (2015). ChRIS–A web-based neuroimaging and informatics system for collecting, organizing, processing, visualizing and sharing of medical data. *Conference Proceedings IEEE Engineering in Medicine and Biology Society*, *2015*, 206–209.

Raij, T., Ahveninen, J., Lin, F.-H., Witzel, T., Jääskeläinen, I. P., Letham, B., Israeli, E., Sahyoun, C., Vasios, C., Stufflebeam, S., Hämäläinen, M., & Belliveau, J. W. (2010). Onset timing of cross-sensory activations and multisensory interactions in auditory and visual sensory cortices. *European Journal of Neuroscience*, *31*, 1772–1782. https://doi.org/10.1111/j.1460-9568.2010.07213.x

Re, T. J., Levman, J., Lim, A. R., Righini, A., Grant, P. E., & Takahashi, E. (2016). High-angular resolution diffusion imaging tractography of cerebellar pathways from newborns to young adults. *Brain and Behavior*, *7*, e00589.

Roine, T., Jeurissen, B., Perrone, D., Aelterman, J., Leemans, A., Philips, W., & Sijbers, J. (2014). Isotropic non-white matter partial volume effects in constrained spherical deconvolution. *Frontiers in Neuroinformatics*, *2014*(8), 28.

Roosendaal, S., Geurts, J., Vrenken, H., Hulst, H., Cover, K., Castelijns, J., Pouwels, P., & Barkhof, F. (2009). Regional DTI differences in multiple sclerosis patients. *NeuroImage*, *44*, 1397–1403. https://doi.org/10.1016/j.neuroimage.2008.10.026

Ross, E. D. (2008). Sensory-specific amnesia and hypoemotionality in humans and monkeys: Gateway for developing a hodology of memory. *Cortex*, *44*, 1010–1022. https://doi.org/10.1016/j.cortex.2008.02.002

Rudrauf, D., David, O., Lachaux, J.-P., Kovach, C. K., Martinerie, J., Renault, B., & Damasio, A. (2008). Rapid interactions between the ventral visual stream and emotion-related structures rely on a two-pathway architecture. *Journal of Neuroscience*, *28*, 2793–2803. https://doi.org/10.1523/JNEUROSCI.3476-07.2008

Sadato, N., Okada, T., Honda, M., Matsuki, K.-I., Yoshida, M., Kashikura, K.-I., Takei, W., Sato, T., Kochiyama, T., & Yonekura, Y. (2005). Cross-modal integration and plastic changes revealed by lip movement, random-dot motion and sign languages in the hearing and deaf. *Cerebral Cortex*, *15*, 1113–1122. https://doi.org/10.1093/cercor/bhh210

Shibata, D. K. (2007). Differences in brain structure in deaf persons on MR imaging studied with voxel-based morphometry. *American Journal of Neuroradiology*, *28*, 243–249.

Shiohama, T., Levman, J., Vasung, L., & Takahashi, E. (2020). Brain morphological analysis in PTEN hamartoma tumor syndrome. *American Journal of Medical Genetics, Part A*, *182*, 1117–1129.

Shiohama, T., McDavid, J., Levman, J., & Takahashi, E. (2019a). The left lateral occipital cortex exhibits decreased thickness in children with sensorineural hearing loss. *International Journal of Developmental Neuroscience*, *76*, 34–40. https://doi.org/10.1016/j.ijdevneu.2019.05.009

Shiohama, T., McDavid, J., Levman, J., & Takahashi, E. (2019b). Quantitative brain morphological analysis in CHARGE syndrome. *NeuroImage Clinical*, *23*, 101866. https://doi.org/10.1016/j.nicl.2019.101866

Takahashi, E., Folkerth, R. D., Galaburda, A. M., & Grant, P. E. (2012). Emerging cerebral connectivity in the human fetal brain: An MR tractography study. *Cerebral Cortex*, *22*, 455–464. https://doi.org/10.1093/cercor/bhr126

Takahashi, E., Hayashi, E., Schmahmann, J. D., & Grant, P. E. (2014). Development of cerebellar connectivity in human fetal brains revealed by high angular resolution diffusion tractography. *NeuroImage*, *96*, 326–333. https://doi.org/10.1016/j.neuroimage.2014.03.022

Thiebaut de Schotten, M., ffytche, D. H., Bizzi, A., Dell'Acqua, F., Allin, M., Walshe, M., Murray, R., Williams, S. C., Murphy, D. G. M., & Catani, M. (2011). Atlasing location, asymmetry and inter-subject variability of white matter tracts in the human brain with MR diffusion tractography. *NeuroImage*, *54*, 49–59. https://doi.org/10.1016/j.neuroimage.2010.07.055

Tomblin, J. B., Walker, E. A., McCreery, R. W., Arenas, R. M., Harrison, M., & Moeller, M. P. (2015). Outcomes of children with hearing loss: Data collection and methods. *Ear and Hearing*, *36*(Suppl 1), 14S–23S. https://doi.org/10.1097/AUD.0000000000000212

Tuch, D. S., Reese, T. G., Wiegell, M. R., Makris, N., Belliveau, J. W., & Wedeen, V. J. (2002). High angular resolution diffusion imaging reveals intravoxel white matter fiber heterogeneity. *Magnetic Resonance in Medicine*, *48*, 577–582. https://doi.org/10.1002/mrm.10268

Turgeon, C., Champoux, F., Lepore, F., & Ellemberg, D. (2012). Reduced visual discrimination in cochlear implant users. *NeuroReport*, *23*, 385–389. https://doi.org/10.1097/WNR.0b013e3283525af4

Vetter, P., Smith, F. W., & Muckli, L. (2014). Decoding sound and imagery content in early visual cortex. *Current Biology*, *24*, 1256–1262. https://doi.org/10.1016/j.cub.2014.04.020

Vishwas, M. S., Healy, B. C., Pienaar, R., Gorman, M. P., Grant, P. E., & Chitnis, T. (2013). Diffusion tensor analysis of pediatric multiple sclerosis and clinically isolated syndromes. *American Journal of Neuroradiology*, *34*, 417–423. https://doi.org/10.3174/ajnr.A3216

Vos, S. B., Jones, D. K., Viergever, M. A., & Leemans, A. (2011). Partial volume effect as a hidden covariate in DTI analyses. *NeuroImage*, *55*, 1566–1576.

Wang, H., Liang, Y. I., Fan, W., Zhou, X., Huang, M., Shi, G., Yu, H., & Shen, G. (2019). DTI study on rehabilitation of the congenital deafness auditory pathway and speech center by cochlear implantation. *European Archives of Oto-Rhino-Laryngology*, *276*, 2411–2417. https://doi.org/10.1007/s00405-019-05477-7

Wang, S., Chen, B., Yu, Y., Yang, H., Cui, W., Li, J., & Fan, G. G. (2019). Alterations of structural and functional connectivity in profound sensorineural hearing loss infants within an early sensitive period: A combined DTI and fMRI study. *Developmental Cognitive Neuroscience*, *38*, 100654. https://doi.org/10.1016/j.dcn.2019.100654

Watanabe, H., Homae, F., Nakano, T., Tsuzuki, D., Enkhtur, L., Nemoto, K., Dan, I., & Taga, G. (2013). Effect of auditory input on activations in infant diverse cortical regions during audiovisual processing. *Human Brain Mapping*, *34*, 543–565.

Wilkinson, M., Lim, A. R., Cohen, A. H., Galaburda, A. M., & Takahashi, E. (2017). Detection and growth pattern of arcuate fasciculus from newborn to adult. *Frontiers in Neuroscience*, *11*, 389. https://doi.org/10.3389/fnins.2017.00389

Wu, C., Huang, L., Tan, H., Wang, Y., Zheng, H., Kong, L., & Zheng, W. (2016). Diffusion tensor imaging and MR spectroscopy of microstructural alterations and metabolite concentration changes in the auditory neural pathway of pediatric congenital sensorineural hearing loss patients. *Brain Research*, *1639*, 228–234.

Xu, G., Takahashi, E., Folkerth, R. D., Haynes, R. L., Volpe, J. J., Grant, P. E., & Kinney, H. C. (2014). Radial coherence of diffusion tractography in the cerebral white matter of the human fetus: Neuroanatomic insights. *Cerebral Cortex*, *24*, 579–592.

Yoshinaga-Itano, C., Sedey, A. L., Wiggin, M., & Chung, W. (2017). Early hearing detection and vocabulary of children with hearing loss. *Pediatrics*, *140*, pii:e20162964.

How to cite this article: Shiohama T, Chew B, Levman J, Takahashi E. Quantitative analyses of high-angular resolution diffusion imaging (HARDI)-derived long association fibers in children with sensorineural hearing loss. *Int J Dev Neurosci*. 2020;80:717–729. https://doi.org/10.1002/jdn.10071